Journal of Applied Polymer Science

Nanocomposites of Ethylene Vinyl Alcohol Copolymer with Thermally Resistant Cellulose Nanowhiskers by Melt Compounding (I): Morphology and Thermal Properties

Marta Martínez-Sanz, Amparo Lopez-Rubio, Jose M. Lagaron
Novel Materials and Nanotechnology Group, IATA, CSIC, 46980 Paterna (Valencia), Spain
Correspondence to: J. M. Lagaron (E-mail: lagaron@iata.csic.es)

ABSTRACT: In this study, ethylene-vinyl alcohol copolymer (EVOH) nanocomposites were prepared by melt compounding both plant cellulose nanowhiskers (CNW) and bacterial cellulose nanowhiskers (BCNW) as nanofillers. Electrospinning and a "dissolution precipitation" method were used as strategies for the incorporation of CNW in EVOH before melt compounding with the aim of enhancing the degree of dispersion of the nanocrystals when compared with direct melt-mixing of the freeze-dried product with the polymer. As revealed by morphological characterization, the proposed preincorporation methods led to a significant improvement in the dispersion of the nanofiller in the final nanocomposite films. Furthermore, it was possible to incorporate concentrations as high as 4 wt % BCNW without causing significant agglomeration of the nanofiller, whereas increasing the CNW concentration up to 3 wt % induced agglomeration. Finally, DSC studies indicated that the crystalline content was significantly reduced when the incorporation method led to a poor dispersion of the nanocrystals, whereas high-nanofiller dispersion resulted in thermal properties similar to those of the neat EVOH. © 2012 Wiley Periodicals, Inc. J. Appl. Polym. Sci. 000: 000–000, 2012

KEYWORDS: biodegradable; biopolymers and renewable polymers; cellulose and other wood products

Received 14 June 2012; accepted 3 August 2012; published online
DOI: 10.1002/app.38433

INTRODUCTION

The great interest of using materials obtained from renewable sources, on which currently many efforts are being focused, is one of the reasons why the use of cellulosic materials as reinforcement agents in nanocomposites has recently gained so much attention. Cellulose is one of the most abundant biopolymers found in nature, and it is commonly extracted from vegetal resources such as wood, cotton, and linter. However, it can also be synthesized by some bacterial species, such as *Gluconacetobacter xylinus*, which, in a culture medium rich in polysaccharides, are able to produce a layer of bacterial cellulose (BC). Compared to plant-derived cellulose (PC), BC shows a finer web-like network structure, higher water holding capacity, and higher crystallinity.[1,2]

For their application in nanocomposites, cellulosic materials are commonly subjected to acid hydrolysis, breaking down the hierarchical structure of the material into crystalline nanofibers or nanocrystals, usually known as cellulose nanowhiskers (CNW). The hydrolysis conditions strongly influence the morphology of the extracted CNW and their aspect ratio (L/D), which has a remarkable influence on the reinforcing capacity when incorporating the nanofiller into a polymeric matrix.[3] In addition to the hydrolysis conditions, the cellulose source has an important effect on the morphology of the obtained nanowhiskers. Although CNW extracted from vegetal resources typically have a length of 100–300 nm and a width of 5–20 nm,[4,5] those obtained from bacterial cellulose (BCNW) may have several micrometers in length and a width of 5–50 nm.[6,7]

Because of their fully degradable and renewable character and good mechanical properties, the use of CNW as reinforcing fillers for polymeric matrixes has grown considerably. Plant-derived CNW have been incorporated into a wide variety of materials, specifically biopolymers such as poly(lactic acid) (PLA),[8,9] poly(3-hydroxybutyrate-*co*-3-hydroxyvalerate),[10] starch,[11] and cellulose acetate butyrate.[12] Solution casting has been the most widely used technique for the incorporation of CNW. Nevertheless, very few reports exist on the production of nanocomposites reinforced with CNW via conventional industrial thermoplastic processing techniques, such as melt-compounding methods. When aiming at the development of nanocomposite materials through melt compounding, one of the main issues is to achieve a good dispersion of the nanofiller within the matrix. An attempt to prepare nanocomposites of PLA reinforced with CNW by pumping a suspension of CNW in DMAc/LiCl into the polymer melt during the extrusion process was reported.[13] Nevertheless,

aggregation and thermal degradation took place to a certain extent. Thermogravimetric analyses (TGA) showed that DMAc/LiCl was responsible for the decreased thermal stability of CNW, which degraded during melt processing. The so-obtained nanocomposites did not show any improvement on the mechanical properties when compared with pure PLA. However, this was due to decreased mechanical properties of PLA when processed with DMAc/LiCl. Compared to PLA treated with DMAc/LiCl, CNW had a positive effect on the mechanical properties of PLA, increasing both the elastic modulus and the elongation at break. Subsequently, the possibility of using poly(vinyl alcohol) (PVA) as a compatibilizer for the nanowhiskers was investigated, but a poor dispersion of them was observed in the PLA matrix.[14] On the other hand, the use of an anionic surfactant effectively enhanced CNW dispersion in PLA by extrusion hence increasing both tensile strength and elongation at break. However, the addition of the surfactant caused PLA thermal degradation.[15] CNW were also incorporated into PHBV by melt processing.[16] Despite using polyethylene glycol as a compatibilizer, CNW could not be homogeneously dispersed within the matrix, and PHBV/CNW composites exhibited decreased strength. More recently, surface grafting of poly(ε-caprolactone) to cellulose nanocrystals by ring-opening polymerization has been reported.[17] PCL-grafted CNW were highly dispersed when incorporated into PCL by melt blending, resulting in improved thermomechanical properties.

In comparison with plant-derived CNW, the use of BCNW is relatively recent, and it has been less frequently addressed in the literature.[18–26] Nevertheless, this material presents excellent properties, which make it very attractive as a nanofiller. Transparent composites of acrylic and epoxy resins reinforced with up to 70% BC nanofibers showed a low-thermal expansion coefficient and mechanical strength five times that of engineered plastics.[27] Electrospinning has been investigated for the incorporation of BCNW into poly(ethylene oxide),[24] poly(methyl methacrylate),[23] and ethylene-vinyl alcohol (EVOH) copolymers.[21,22] A previous work[21] suggested the use of electrospinning as a vehicle for the incorporation of highly dispersed nonthermally stable BCNW into EVOH. It was demonstrated how this methodology of incorporating BCNW within electrospun structures led to relatively higher stability and dispersion of the BCNW compared to the direct addition of the freeze-dried nanofiller to the matrix. Nevertheless, the low-thermal stability of the nonthermally stabilized nanofiller gave rise to a certain degree of degradation during melt compounding of the material.

In this first study of a series of two works, the use of the electrospinning technique, as well as a solution-precipitation method, was proposed as means of incorporating homogeneously distributed thermally stable BCNW and also plant CNW into an EVOH matrix. The purpose of this work was to improve the dispersion of the highly optimized BCNW filler in the polymeric material obtained after a subsequent melt-mixing step. In this first work, the morphology and thermal properties of films obtained through the cited and proprietary methods[28,29] were studied and compared to the films produced by direct melt-mixing of the thermally stabilized freeze-dried cellulosic material. The effect of the nanofiller loading in the morphology of the nanocomposites was also evaluated. Finally, a comparative study between films incorporating BCNW and CNW was performed to determine the influence of the cellulose source in the properties of the obtained nanocomposites. In a second study, the mechanical and barrier properties of the produced nanocomposites will be presented and discussed.

MATERIALS AND METHODS

Materials

EVOH grade (Soarnol) EVOH32 (containing 32 mol % of ethylene) was supplied by The Nippon Synthetic Chemical Industry Co. (NIPPON GOHSEI) (Japan). Sulfuric acid 96% and 2-propanol were purchased from Panreac (Barcelona, Spain).

BC mats were obtained following a procedure similar to the one described in a previous work[22] and supplied by BioInicia S.L. (Valencia, Spain).

For the production of plant CNW, a purified cellulose microfiber (CMF) grade from CreaFill Fibers Corp. (USA), having an average fiber length of 60 μm and an average fiber width of 20 μm, was used as a raw material. According to the manufacturer's specifications, these fibers had an α-cellulose content in excess of 99.5%.

Preparation of Heat-Stable BC Nanowhiskers

Bacterial cellulose (BC) pellicles were ground in a blender, and the gel-like material was then compressed in order to remove most of the absorbed water. The dried material was then treated with 301 mL sulfuric acid/L water in a cellulose/acid ratio of ~7 g/L at 50°C for 3 days until a homogeneous solution was obtained. The CNWs were obtained as a white precipitate after several centrifugation and washing cycles at 12,500 rpm and 15°C for 20 min. After that, the material was resuspended in deionized water and neutralized with sodium hydroxide until neutral pH and, subsequently, centrifuged to obtain the final product as a partially hydrated precipitate. This last step is thought to turn the filler heat stable. The humidity of the material was determined, and the yield of the extraction process was estimated to be ~80% with respect to the dried BC. The product was kept refrigerated, and one fraction was freeze-dried for further analyses.

Preparation of Plant Cellulose Nanowhiskers

Highly purified α-CMF were hydrolyzed in 9.1 mol/L sulfuric acid, in a 10 g/100 mL cellulose/acid ratio, at 37°C for 130 min, as previously described in the literature.[9,16] After several centrifugation cycles, the turbid supernatant containing CNW was collected and subjected to neutralization, followed by dialysis. Subsequently, the suspension was freeze-dried thus obtaining the CNW. The yield of the process was ~5% with respect to the raw α-cellulose.

Electrospinning

Electrospun hybrid fibers were generated by using 5% (w/v) EVOH solutions in 70/30 (v/v) 2-propanol/water. Both pure EVOH and the EVOH solutions containing a concentration of 15% (w/w) BCNW with regard to the EVOH weight were used to generate electrospun fibers. BCNWs, in the form of a partially hydrated precipitate, were dispersed in the solvent by intense homogenization (Ultra-turrax). The optimization of this process was carried out in previous works.[21,22]

The electrospinning apparatus was a FluidnaTek® basic equipment manufactured by the engineering division of BioInicia S.L. (Valencia, Spain). Solutions were transferred to 5-mL plastic syringes and connected through PTFE tubes to a stainless steel needle (Ø 0.9 mm). An electrode was clamped to the needle tip and connected to a high-voltage 0–30 kV power supply operating at 12–14 kV, and polymer solution was fed into the needle at a rate of 0.6 mL/h by a syringe pump (KD Scientific, Holliston, USA). The counter electrode was connected to a rectangular plate covered by aluminum foil, which was placed parallel to the needle to collect the electrospun fibers. The distance between the needle and the plate was set at 11 cm, and experiments were carried out at ambient temperature.[30]

Preparation of Films

EVOH nanocomposite films were prepared using three different methods: the traditional method of directly melt-mixing the polymeric matrix with the freeze-dried nanofiller and two other patent-pending methods[28,29] of incorporating CNW into the EVOH matrix, previous to the melt-compounding stage, as explained below.

The first method consisted in the incorporation of CNW into EVOH32 fibers by means of the electrospinning technique. Electrospun EVOH fibers containing 15% (w/w) BCNW were melt-mixed with virgin EVOH32 pellets in order to obtain a diluted composite having a final concentration of 2 wt % BCNW (sample code: 2% BCNW ES).

The second method involved the preparation of EVOH32 solutions containing a 15% (w/w) of CNW or BCNW. Partially hydrated BCNW and freeze-dried CNW were dispersed in water by means of homogenization (Ultra-turrax) and sonication. This aqueous dispersion was mixed with 2-propanol, so that the final ratio was 70/30 (v/v) 2-propanol/water, and a 5% (w/v) EVOH was dissolved together with the nanowhiskers. These solutions were then quenched and precipitated by adding liquid nitrogen, and the obtained product was then dried at 60°C until complete evaporation of the remaining solvent and subsequently ground into a powder. This powder was then used to produce films by melt-mixing the adequate amount of it with virgin EVOH32 pellets in order to obtain films containing 1, 2, and 3 wt % CNW (sample codes: 1% CNW FD-P, 2% CNW FD-P, and 3% CNW FD-P) and 1, 2, 3, and 4 wt % BCNW (sample codes: 1% BCNW P, 2% BCNW P, 3% BCNW P, and 4% BCNW P). Additionally, films containing 2 wt % of freeze-dried BCNWs and BC were prepared by repeating the same process as described immediately above (sample codes: 2% BCNW FD-P and 2% BC FD-P, respectively).

Regarding the traditional method, films containing 2 wt % of CNW and BCNW were produced by melt-mixing the freeze-dried material with the required amount of EVOH32 pellets (sample codes: 2% CNW FD and 2% BCNW FD, respectively).

All the blends were prepared in a Brabender Plastograph mixer during 3 min at 100 rpm and 185°C. The batches were subsequently compression molded into films using a hot-plate hydraulic press (180°C and 2 MPa for 4 min) and rapidly cooled down using air and water. The films produced had a thickness of ~100 μm, and each film was characterized using a Mitutoyo micrometer by averaging four measurements.

Scanning Electron Microscopy

Scanning electron microscopy (SEM) was conducted on a Hitachi microscope (Hitachi S-4100) at an accelerating voltage of 10–15 kV and a working distance of 12–16 mm. Electrospun fibers and films cryofractured after immersion in liquid nitrogen were sputtered with a gold–palladium mixture under vacuum before their morphology was examined using SEM. Fiber diameters of the electrospun fibers were measured by means of the Adobe Photoshop CS3 extended software from the SEM micrographs in their original magnification.

Transmission Electron Microscopy

One drop (8 μL) of a 0.001% aqueous suspension of CNW and BCNW was allowed to dry on a carbon-coated grid (200 mesh). The crystals were stained with a 2 wt % solution of uranyl acetate. Additionally, ultrathin sections of microtomed composite sheets were observed through TEM. The samples were also stained with uranyl acetate. TEM was performed using a JEOL 1010 equipped with a digital Bioscan (Gatan) image acquisition system at 80 kV.

Transmission and Attenuated Total Reflectance FTIR analysis

Transmission FTIR experiments were recorded in a controlled chamber at 21°C and 40% RH using a Bruker (Rheinstetten, Germany) FTIR Tensor 37 equipment. The spectra were taken at 1 cm^{-1} resolution averaging a minimum of 10 scans. Analysis of the spectra was performed using Grams/AI 7.02 (Galactic Industries, Salem, NH) software. Samples of ~2 mg of electrospun fibers were ground and dispersed in 200 mg of spectroscopic grade KBr. A pellet was then formed by compressing the sample at ~150 MPa. A calibration curve was obtained by recording the IR spectra of pellets containing 6 mg of EVOH-BC nanowhiskers samples with nanowhiskers' concentrations ranging from 10 to 40 wt %. The detailed procedure can be found elsewhere.[22] Briefly, the intensity of the band at 1165 cm^{-1}, which was chosen as characteristic for cellulose, was divided by the intensity of the band at 838 cm^{-1}, which was assigned to the EVOH contribution. Subsequently, the IR spectra of the electrospun fibers were analyzed, and the percentages of BCNW incorporated into the fibers from the solutions were estimated.

ATR–FTIR spectra of CMF, BC, CNW, BCNW, and all the obtained films were collected in the same environmental conditions as the transmission experiments, coupling the ATR accessory GoldenGate of Specac (Orpington, UK) to the above-mentioned FTIR equipment. All spectra were recorded by averaging 20 scans at 4 cm^{-1} resolution.

X-Ray Diffraction

X-ray diffraction was carried out on a D5005 Bruker diffractometer. The instrument was equipped with a Cu tube and a secondary monochromator. The samples were examined over the angular range of 5°–45° with a step size of 0.02° and a count time of 4 s per point.

Peak fitting was carried out using Igor software package (Wavemetrics, Lake Oswego, OR). Gaussian function was used to fit the experimental diffraction profiles obtained. For the fitting procedure, the reflections considered were (i) three at 14.8°, 16.4°, and 22.5° 2θ (corresponding to the 101, $10\bar{1}$, and 002 crystal planes, respectively) assigned to the cellulose I allomorph and (ii) the amorphous halo centered at ~18.5° 2θ. The crystallinity index CI (XD) was determined by the method reported by Wang et al.:[31]

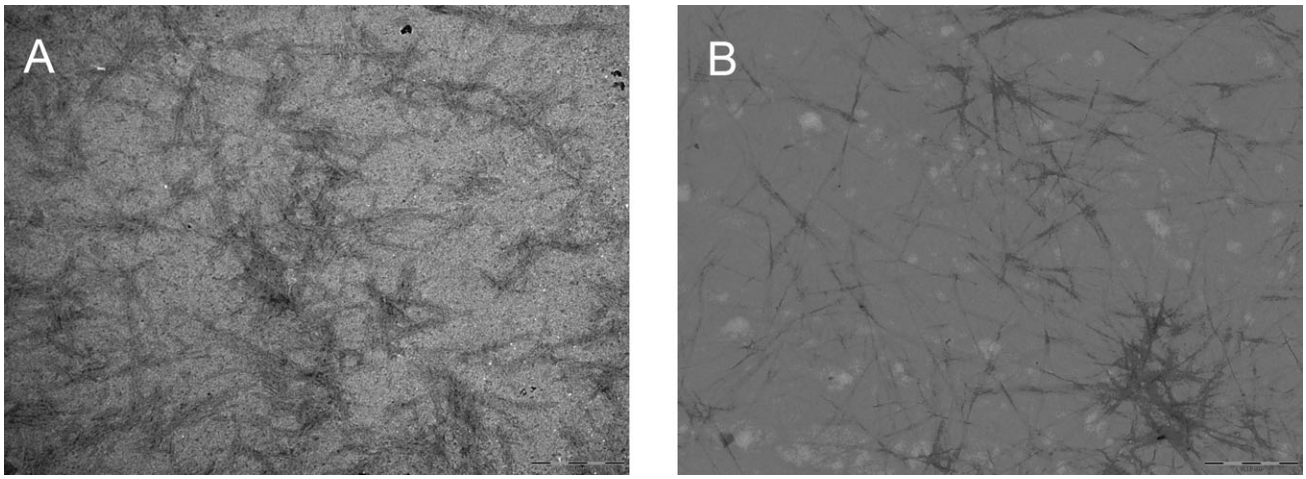

Figure 1. TEM micrographs of CNW (A) and BCNW (B). Scale markers correspond to 1000 nm in picture (A) and 500 nm in picture (B).

$$\mathrm{CI(XD)} = \frac{\sum A_{\mathrm{Crystal}}}{A_{\mathrm{Total}}} \times 100$$

where A_{Total} is the sum of the areas under all the diffraction peaks and $\Sigma A_{\mathrm{Crystal}}$ is the sum of the areas corresponding to crystalline peaks.

The crystallite sizes were estimated from the 101, $10\bar{1}$, and 002 lattice planes of cellulose I using the well-known Scherrer equation:

$$D_{(hkl)} = \frac{k \cdot \lambda}{B_{(hkl)} \cdot \cos\theta}$$

where $D_{(hkl)}$ is the size of the crystallite (nm), k is the Scherrer constant (0.94), λ is the X-ray wavelength, $B_{(hkl)}$ is the full-width at half-maximum of the reflection hkl, and 2θ is the corresponding Bragg angle.

Differential Scanning Calorimetry

DSC experiments were carried out in a Perkin-Elmer DSC-7 calorimeter. The sample treatment consisted of a first-heating melting step from 30 to 220°C, a subsequent cooling down to 30°C, and a second-heating melting step up to 220°C. The heating and cooling rates for the runs were 10°C/min, and the typical sample weight was around 3 mg. Calibration was performed using an indium sample, and the slope of the thermal scans was corrected by subtracting similar scans of an empty pan. All tests were carried out, at least, in duplicate.

The crystallinity (%) of the EVOH was estimated from the corrected enthalpy for the EVOH content in the nanocomposites, using the ratio between the enthalpy of the studied material and the enthalpy of a perfect EVOH crystal, that is, $X_c(\%) = \frac{\Delta H_f}{\Delta H_f^0} \times 100$, where ΔH_f is the enthalpy of fusion of the studied specimen and ΔH_f^0 is the enthalpy of fusion of a totally crystalline material. The ΔH_f^0 used for this equation was 216.6 J/g for the EVOH.[32]

Thermogravimetric Analysis

Thermogravimetric (TG) curves were recorded with a TA Instruments model Q500 TGA. The samples (~20 mg) were heated from 50 to 600°C at a heating rate of 10°C/min under nitrogen atmosphere. Derivative TG curves (DTG) express the weight loss rate as a function of temperature.

RESULTS AND DISCUSSION

Characterization of Bacterial and Plant Cellulose Nanowhiskers

The overall objective of this study was to optimize the dispersion of the cellulosic nanofillers in the polymeric matrix when producing films by the melt-compounding technique. In addition to different pre-incorporation methods, the effects of the nanowhiskers' loading and of the cellulose source on the thermal properties of the materials were also evaluated in this first study.

The morphology of the two different nanofillers used in this work, that is, plant CNW and BCNW, obtained through sulfuric acid hydrolysis, was studied by TEM (cf. Figure 1). BCNWs were extracted by the optimized method developed in a previous work[33] and showed the same morphology as observed earlier, with an average cross-section of ~18 nm and length of ~570 nm. On the other hand, the CNWs extracted by the standard extraction method[8,9] displayed a morphology of shorter whiskers of ~287 nm length and ~24 nm cross-section, which were aggregated to a greater extent, because they had been previously subjected to a freeze-drying process, which was not applied to the BCNWs. Furthermore, the length of the produced CNWs was in the same range as that previously reported after using similar extraction procedures,[8,34] but with a wider cross-section, probably because the applied hydrolysis temperature was lower than that reported in previous works.

The expected increase in the overall crystallinity of the resulting nanowhiskers as a result of the sulfuric acid digestion of the native bacterial or plant cellulose was assessed by XRD and FTIR analyses.

The XRD patterns of BC, plant CMF, and the corresponding nanowhiskers obtained after acid treatment are shown in Figure 2. In the case of BC, three major diffraction peaks were observed at 14.5°, 16.4°, and 22.5° 2θ which, according to the literature,[35] are ascribed to the cellulose I crystallographic planes

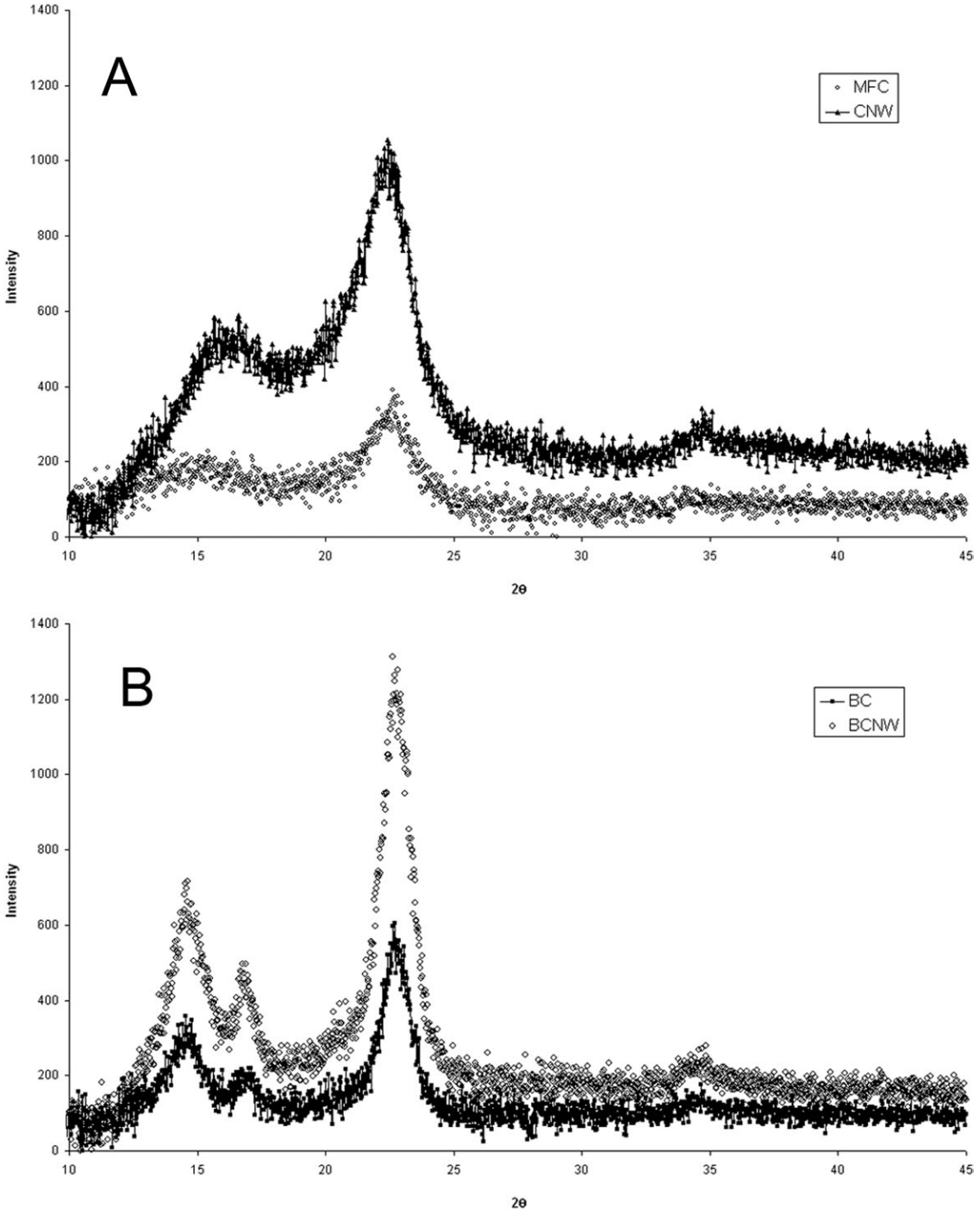

Figure 2. X-ray diffraction patterns of (A) plant cellulose microfibers (MFC) and the extracted cellulose nanowhiskers (CNW) and (B) bacterial cellulose (BC) and bacterial cellulose nanowhiskers (BCNW).

101, $10\bar{1}$, and 002, respectively. On the other hand, the diffraction patterns obtained for the plant microfibers and nanowhiskers correspond to those previously reported for PC,[34,36] showing one major diffraction peak located at 22° 2θ and a shoulder in the region 14°–17° 2θ. Crystallinity indexes and crystallite sizes determined from the XRD data are compiled in Table I. As expected, the applied acid hydrolysis produced an increase of 16–19% in the crystallinity index of both materials. Additionally, the average crystallite size calculated from the crystalline planes of cellulose I increased after the hydrolysis, thus suggesting that smaller and/or more defective crystals were hydrolyzed during the acid treatment (cf. Table I). BC presented a crystallinity value similar to that previously reported for BC with[37] and without[22,38] sonication treatment, whereas BCNW obtained through the optimized method applied in this work presented higher crystallinity index than that reported for less

Table I. Crystallinity Index [CI (XD)] and Crystallite Sizes ($D_{(101)}$,$D_{(10\bar{1})}$, and $D_{(002)}$) Determined from the XRD Patterns of Native Cellulose Microfibers (CMF) and Bacterial Cellulose (BC) and of the Obtained Nanowhiskers (CNW and BCNW)

	CMF	CNW	BC	BCNW
CI (XD) (%)	41.4 (0.1)	60.2 (0.1)	79.1 (0.4)	95.3 (0.3)
$D_{(101)}$(nm)	0.5 (0.0)	1.0 (0.0)	0.8 (0.0)	1.0 (0.0)
$D_{(10\bar{1})}$(nm)	-	-	1.7 (0.1)	1.6 (0.0)
$D_{(002)}$(nm)	0.7 (0.0)	0.8 (0.0)	1.1 (0.0)	1.2 (0.0)

severe acid hydrolysis conditions.[38] On the other hand, plant CNW presented a crystallinity index lower than that reported for microcrystalline cellulose (~87%)[37] or nanowhiskers extracted from Avicel (~81%),[39] because the raw CMF used in this work presented lower crystallinity than the raw materials used in the mentioned studies. It is worth noting that the crystallinity index of BC was noticeably higher than that of the PC microfibers, hence highlighting the convenience of BC when aiming at obtaining highly crystalline whiskers.

Additionally, differences in crystallinity between bacterial and PC were evaluated by means of ATR–FTIR analyses. The shape of the bands at 4000–2995 cm^{-1}, 2900 cm^{-1}, 1430 cm^{-1}, 1375 cm^{-1}, and 900 cm^{-1} has been previously related to the amount of crystalline versus amorphous fractions in cellulose, that is, broadening of these bands was related to greater molecular disorder in the polysaccharide phase morphology.[40] From Figure 3, it can be observed that the intensity of these bands was higher in the case of BC and, moreover, that the applied acid treatments gave rise to an increase in the crystallinity of both materials. Therefore, in agreement with the XRD results, the efficiency of the sulfuric acid treatments and the higher crystallinity of BC are confirmed.

The thermal stability of the obtained nanocrystals was studied through TGA. As shown in Figure 4, BCNW presented greater thermal stability than CNW. Degradation began at 186°C for the CNW, whereas the onset temperature for BCNW was 226°C. This increased thermal stability of BCNW was probably a result of its higher crystallinity. Nevertheless, none of the materials underwent thermal degradation at 185°C, which was the temperature applied during the melt-mixing processing of the materials for the production of nanocomposite films. It has been previously demonstrated that the neutralization step applied after the acid treatment is essential for obtaining a more thermally stable material. No mention to neutralization is provided in most of the literature dealing with CNW.[4,10,12,41] From our experience, even after extensive washing cycles, if neutralization is not applied, the material remains acid.[21,33] However, this may not have been a noticeable issue, because solution casting has been the main processing method for this filler in most of the existing literature. Thus, the greater thermal stability achieved for the cellulose nanofillers is one of the differentiating features of this work compared to previous published results.

Various strategies were developed in this work to obtain EVOH films incorporating thermally stable CNW and to ascertain the most suitable incorporation method, which leads to a better dispersion of the nanofiller. Because bacterial and plant-derived CNW presented differences in crystallinity, morphology, and thermal properties, EVOH films with different characteristics were expected to be obtained when incorporating them as nanofillers. The following part of this study deals with the morphological and thermal characterization of the polymeric films obtained through the different incorporation methods using both reinforcing materials.

It should be noted that previous works[21,22] published by our group that made use of BCNW were carried out with a less stable form of BCNW (not neutralized BCNW) and, therefore, this study reports for the first time on the morphology and properties of EVOH nanocomposites containing thermally stable BCNW. EVOH is a relatively high-temperature processing polymer, and, therefore, thermally stable fillers are required when melt-compounding routes are devised. The additional interest in this polymer arises, because it can be solubilized in polar solvents, and, thus, high loadings of water/alcohol dispersible fillers can be incorporated in this polymeric matrix. Moreover, EVOH can undergo melt compounding for later dilution of the filler using conventional plastics melt-processing techniques. So, in a way, it is an excellent carrier for polar nanofillers, which are aimed to be later dispersed into this or into any other polymer matrices to reinforce them.

Nanocomposite EVOH Films Reinforced with BC Nanowhiskers

In the case of bacterial cellulose (BC), two main incorporation methods were developed in order to compare their efficiency in dispersing the nanowhiskers. Both the previously described electrospinning technique and a precipitation method were used. The precipitation method was carried out using both partially hydrated nanowhiskers, just as done for the electrospinning method and, additionally, freeze-dried nanowhiskers (cf.

Table II. DSC Maximum of Melting (T_{m1}), Melting Enthalpy (ΔH_{m1}), and Degree of Crystallinity (X_c) of Neat EVOH and Materials Incorporating 15 wt % BCNW, Obtained from the First Heating Run and Melting Temperature (T_{m2}), Melting Enthalpy (ΔH_{m2}), and Glass Transition Temperature (T_g), Obtained from the Second Heating Run

	T_{m1} (°C)	ΔH_{m1} (J/g EVOH)	X_c (%)	T_{m2} (°C)	ΔH_{m2} (J/g EVOH)	T_g (°C)
EVOH pellets	182.8 ± 0.4	74.8 ± 1.8	34.5 ± 0.8	183.8 ± 0.1	58.4 ± 1.2	60.9 ± 0.3
Electrospun EVOH	184.5 ± 0.4	72.4 ± 2.3	33.4 ± 1.1	183.5 ± 0.5	60.9 ± 3.1	57.6 ± 0.2
Precipitated EVOH+15% BCNW	181.0 ± 0.5	49.0 ± 2.7	22.6 ± 1.2	179.3 ± 0.4	33.7 ± 1.1	58.3 ± 0.2
Electrospun EVOH+15% BCNW	182.9 ± 0.1	91.0 ± 2.1	42.0 ± 1.0	181.9 ± 0.6	67.7 ± 2.6	57.9 ± 0.2

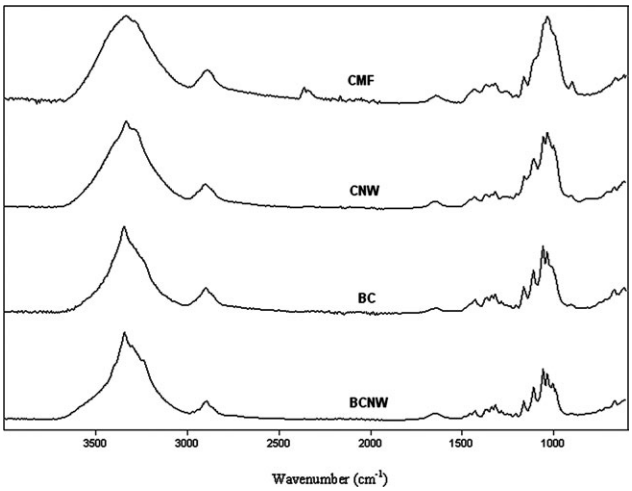

Figure 3. ATR–FTIR spectra of, from top to bottom, cellulose microfibres (CMF), CNW, native bacterial cellulose (BC), and BCNW.

"Materials and Methods" section for more details). The product batches obtained through these methods were then melt-mixed with EVOH in order to obtain films with 2 wt % BCNW and were compared to the traditional method of directly melt-mixing freeze-dried BCNW with EVOH. The reason for using a 2 w % CNW loading was that previous works found it to be the optimum reinforcing level in cellulose-based nanocomposites for barrier enhancement.[9]

With the aim of assessing that the incorporation of BCNW into the EVOH matrix was similar in the case of the electrospinning and precipitation methods, that is, 15 wt % BCNW, FTIR analyses were carried out. Just like in previous works,[21,22] the ratio between the intensity of the band at 1165 cm^{-1} and the band at 838 cm^{-1}, which correspond to the C—O—C asymmetric stretching[42] and to skeletal vibrations and CH_2 rocking of EVOH,[43] respectively, was calculated in order to estimate the BCNWs incorporation degree by applying the previously obtained calibration curve. The obtained spectra are shown in Figure 5, where it is clearly observed how the cellulose characteristic bands, that is, those at 1164, 1111, 1055, and 1035 cm^{-1}, are present both in the electrospun fibers and in the material obtained after precipitation. The estimated BCNWs' incorporation was 15% in the case of the precipitated material, whereas it was ~12% in the case of the electrospun fibers.

Morphology and Thermal Properties of Electrospun and Precipitated Hybrid EVOH-BCNW Materials. The morphology and thermal properties of the materials obtained by the two incorporation methods were analyzed before the melt-mixing step. As observed in Figure 6, the morphology of electrospun fibers was altered by adding BCNW, that is, a more homogeneous and less-beaded fibers were obtained when compared with the pure EVOH fibers. By averaging ~100 measurements of the fibers cross-sections obtained from SEM micrographs, it was observed that the mean diameter of electrospun fibers decreased from 182 ± 79 nm, for pure EVOH fibers, to 132 ± 53 nm when incorporating 15% BCNW. This reduction in the average diameter of electrospun fibers has been previously reported and ascribed to an increase in the conductivity of the electrospinning solution when incorporating CNW.[22,44]

When incorporating neutralized BCNWs, an increase in the melting enthalpy of electrospun fibers was observed compared to pure EVOH fibers, just as deduced from Table II. On the contrary, the melting enthalpy of the material subjected to the precipitation method was noticeably decreased when compared with pure EVOH, because, in this case, the polymeric matrix was quenched, so that the crystallization process of EVOH was impaired.

Morphology of EVOH Nanocomposite Films Containing 2 wt % BCNW. Figure 7 shows the photographs of the obtained EVOH-BCNW films. First, it is observed that all the films produced through the precipitation method presented a similar contact transparency, which was not apparently modified with respect to the pure EVOH film, thus indicating that a good dispersion of the nanofiller must have been achieved. However, the sample with 4 wt % showed a darker color probably due to the high content of the nanofiller. Excellent contact transparency

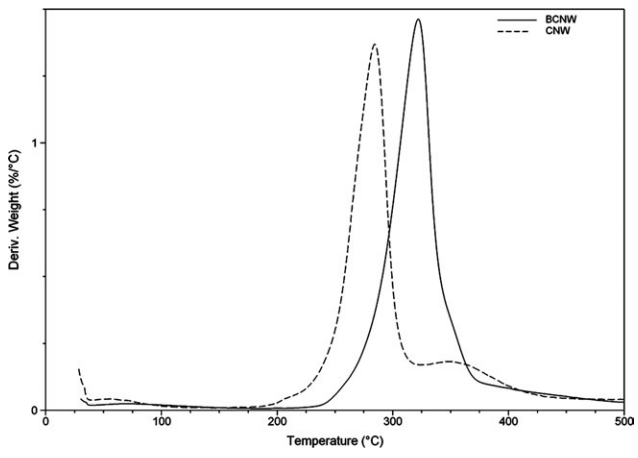

Figure 4. DTG curves of plant cellulose and bacterial cellulose nanowhiskers (CNW and BCNW, respectively).

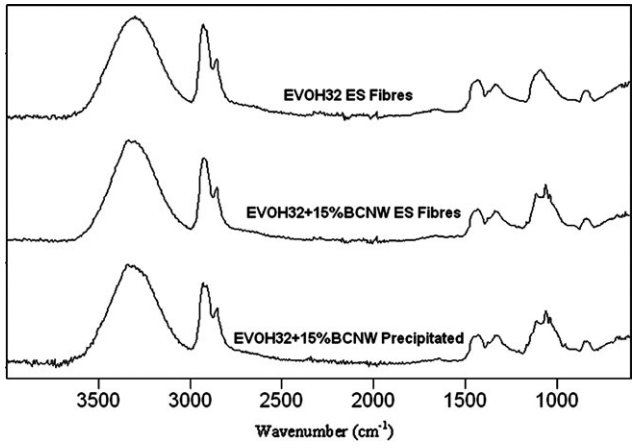

Figure 5. FTIR spectra of electrospun EVOH32 fibers, electrospun EVOH32 fibers containing 15 wt % BCNW and EVOH32 incorporating 15 wt % BCNW by means of the precipitation method.

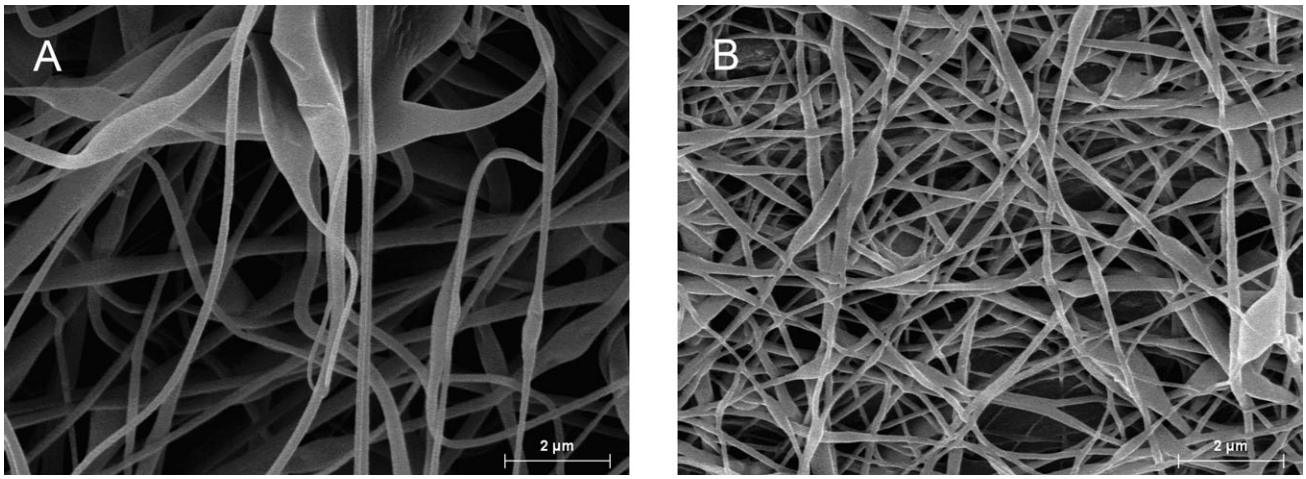

Figure 6. SEM micrographs of electrospun EVOH32 fibers and electrospun EVOH32 fibers containing 15 wt % BCNW.

was also observed for the sample with 2 wt % BCNW incorporated through electrospun fibers. On the other hand, brown spots were observed in the films obtained by the direct addition of freeze-dried BCNW (cf. Figure 7F). Nevertheless, when using the precipitation method for incorporating freeze-dried BCNW (Figure 7E), those brown spots completely disappeared, thus indicating that the dispersion of the nanofiller may be significantly enhanced by this procedure. When using freeze-dried BC microfibers instead of whiskers as the filler, white agglomerates were clearly observed in the obtained films even though the filler was incorporated through the precipitation method (image not shown).

To thoroughly study the morphology and the dispersion of the nanofiller in the nanocomposite films, cryofractured surfaces were observed by SEM. BCNW could be easily identified in Figure 8, because they appeared either as white dots or forming bundles in Figure 8D. The filler seemed to be homogeneously distributed within the matrix presenting a similar morphology to that observed for starch nanocomposites reinforced with tunicin whiskers[45] and for PVA reinforced with cellulose nanofibers.[46]

When comparing the fracture surface of the different 2 wt % samples (Figure 8), the first noticeable observation was that the dispersion of the nanofiller was poor when directly melt-mixing the freeze-dried BCNW with the EVOH matrix. In this specific case, BCNWs were aggregated presenting an average cross-section of 157 nm, and there were some nanowhiskers bundles having cross-sections up to 560 nm. Surprisingly, when applying the precipitation method, the dispersion of the freeze-dried product was significantly improved, presenting a cross-section of 75 ± 26 nm with no visible bundles.

Another interesting result is that the dispersion of the nanofiller was very similar when using both partially hydrated or freeze-dried BCNW and applying the precipitation method. A very good dispersion was also achieved when incorporating 2 wt % BCNW through electrospinning, being the average nanofiller cross-section of 46 ± 14 nm versus 81 ± 20 nm for the samples obtained through the precipitation method.

In any case, the determined cross-sections were much higher than the BCNW's diameter, which could be due to a charge concentration effect caused by the emergence of BCNW from the examined surface.[45] In conclusion, all the developed incorporation methods represented an improvement compared to the direct melt-mixing of freeze-dried BCNW. Even when using untreated freeze-dried BC as the filler, smaller agglomerates were observed, and the dispersion was enhanced by means of the precipitation step.

Effect of BCNW Loading on the Morphology of EVOH Nanocomposites. In addition to the 2 wt % BCNW films, different concentrations of partially hydrated whiskers were incorporated by the precipitation method (1, 3, and 4 wt %

Figure 7. Photographs of films containing: (A) Pure EVOH; (B) EVOH + 2 wt % BCNW precipitated; (C) EVOH + 4 wt % BCNW precipitated; (D) EVOH + 2 wt % BCNW ES; (E) EVOH + 2 wt % BCNW freeze-dried/precipitated, and (F) EVOH + 2 wt % BCNW freeze-dried. [Color figure can be viewed in the online issue, which is available at wileyonlinelibrary.com.]

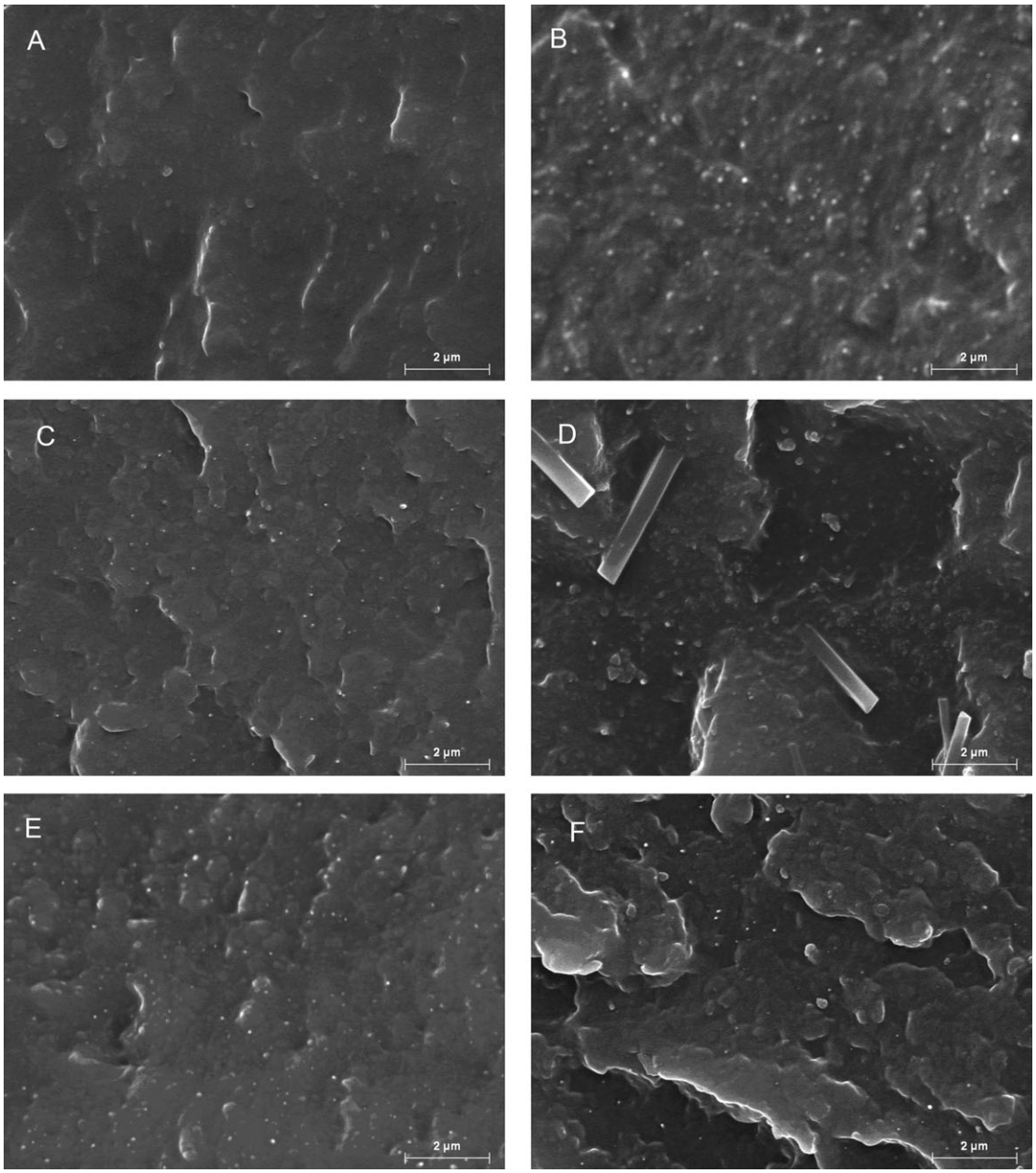

Figure 8. SEM micrographs of the cryofractured section obtained from EVOH films: (A) Pure EVOH; (B) 2% BCNW P; (C) 2% BCNW ES; (D) 2% BCNW FD; (E) 2% BCNW FD-P, and (F) 2% BC FD-P. Scale markers correspond to 2 μm.

BCNW). The ATR–FTIR spectra of all the produced films were recorded, and it was observed that the previously mentioned characteristic bands from cellulose were only apparent for concentrations greater than 3 wt % BCNW (results not shown). It was observed by visual examination of EVOH-BCNW films that the films containing more than 2 wt % BCNW had a yellowish color, but still maintained good optical characteristics (cf. Figure 7C). The effect of increasing the BCNW concentration in the dispersion when applying the precipitation method was studied by TEM. No significant agglomeration effect was observed when increasing the nanofiller concentration up to 4 wt %, as seen in Figure 9. As calculated from the cryo-SEM images (not shown), the BCNW were distributed within the matrix presenting cross-sections of 44 $\pm$ 16 nm, 81 $\pm$ 20 nm, 37 $\pm$ 14 nm, and 44 $\pm$ 35 nm, respectively, for the 1, 2, 3, and 4 wt % precipitated BCNW films.

Thermal Properties of the Various EVOH Nanocomposites Developed with BCNW. With the aim of investigating the effects of the BCNW addition on the thermal properties of the EVOH nanocomposites, DSC analyses of all the samples were carried out. The melting temperature (T_m) and melting enthalpy (ΔHm) normalized to the EVOH content of the nanocomposite films were obtained from the DSC first-heating run, whereas the glass transition temperature (T_g) was determined from the second-heating run (see Table III).

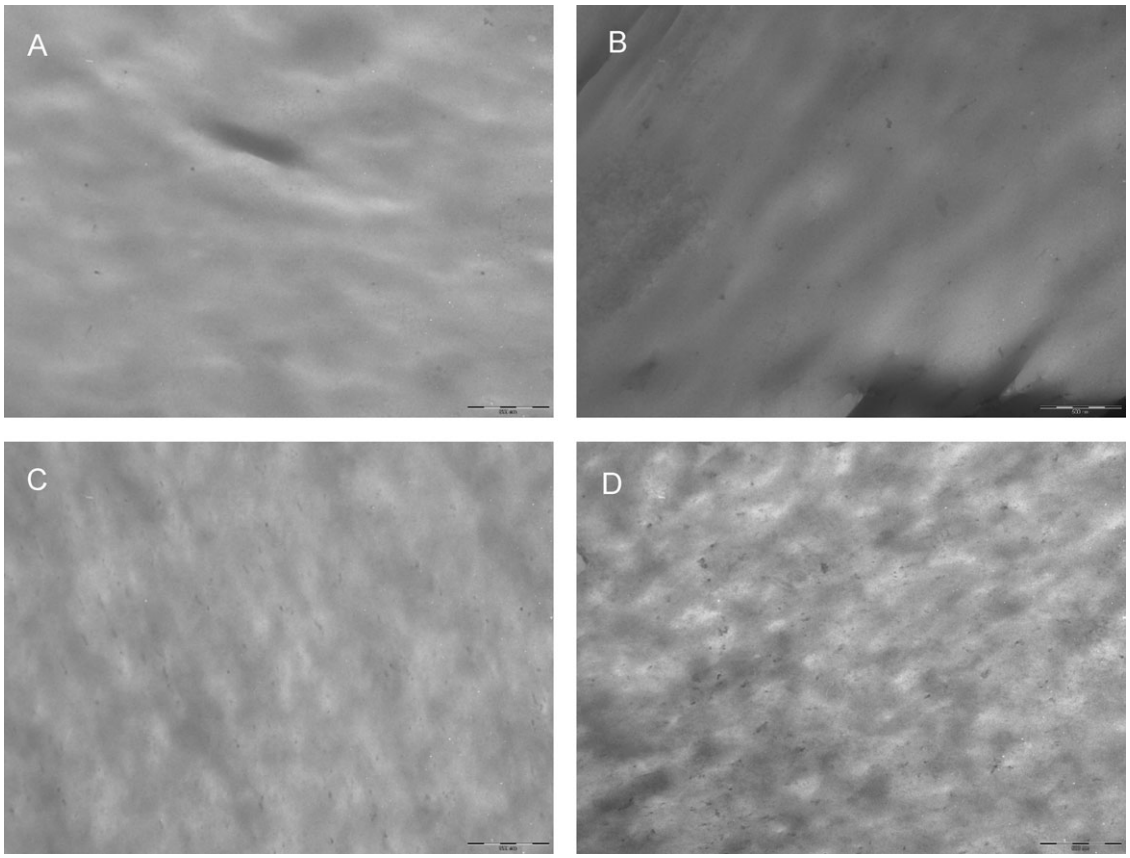

Figure 9. TEM micrographs of EVOH films containing: (A) 1 wt % BCNW precipitated; (B) 2 wt % BCNW precipitated; (C) 3 wt % BCNW precipitated, and (D) 4 wt % BCNW precipitated. Scale markers correspond to 500 nm.

A general trend of decreasing melting enthalpy is observed when incorporating BCNW or BC into the EVOH matrix through melt-mixing, regardless the method of incorporation or the loading amount, thus indicating that the nanofiller is somehow hindering the crystallization process of the polymer. The same result has been previously observed for poly(oxyethylene) reinforced with tunicin CNW and was attributed to an increase in the viscosity of the polymer melt caused by the presence of whiskers, which leads to an increase in the activation energy needed for the diffusion of the chains.[47] Regarding the T_g, no significant changes are produced in comparison with the pure EVOH film.

When comparing the different incorporation methods for a fixed concentration of 2% BCNW, it is observed that the 2% BCNW P and 2% BCNW ES films displayed slightly higher melting temperatures than the rest of the 2% BCNW films, suggesting that bigger or denser EVOH crystals were formed in both cases. However, a decrease in the crystallinity of the films obtained through the precipitation method was observed when compared with the pure EVOH. Similarly, lower crystallinity

Table III. DSC Maximum of Melting (T_m), Melting Enthalpy (ΔHm), Peak Width, and EVOH Crystallinity (X_c) of EVOH Films, Obtained During the First Heating Run and Glass Transition Temperature (T_g), Obtained During the Second Heating Run

	T_m (°C)	ΔH_m (J/g EVOH)	Peak width	X_c (%)	T_g (°C)
EVOH	177.7 ± 1.5	76.5 ± 0.1	7.1 ± 0.5	35.3 ± 0.0	59.5 ± 0.8
1% BCNW P	177.7 ± 0.5	67.0 ± 10.5	7.8 ± 0.2	31.0 ± 4.8	59.9 ± 0.2
2% BCNW P	178.5 ± 0.2	68.9 ± 4.4	7.1 ± 0.4	31.8 ± 2.0	58.6 ± 0.0
3% BCNW P	176.8 ± 0.0	64.4 ± 5.2	7.7 ± 0.1	29.7 ± 2.4	59.7 ± 0.7
4% BCNW P	177.2 ± 0.2	72.1 ± 1.2	9.6 ± 0.0	33.3 ± 0.6	58.7 ± 0.5
2% BCNW ES	178.0 ± 0.0	75.8 ± 2.3	7.3 ± 1.7	35.0 ± 1.1	58.6 ± 0.1
2% BCNW FD	177.4 ± 0.1	71.9 ± 0.9	6.0 ± 0.2	33.2 ± 0.4	58.5 ± 0.1
2% BCNW FD-P	177.9 ± 1.1	75.4 ± 3.2	8.8 ± 0.1	34.8 ± 1.5	60.1 ± 0.3
2% BC FD-P	177.3 ± 0.1	67.2 ± 8.0	8.3 ± 1.1	31.0 ± 3.7	59.9 ± 0.7

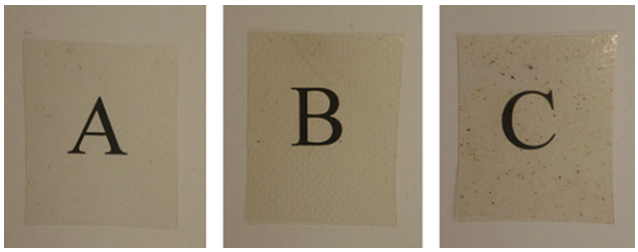

Figure 10. Photographs of films: (A) 1% CNW FD-P; (B) 2% CNW FD-P, and (C) 2% CNW FD. [Color figure can be viewed in the online issue, which is available at wileyonlinelibrary.com.]

values were also observed for the films containing 2% BCNW FD and untreated BC, although it should be emphasized that there was a high variability of the data (compare with standard deviation values) precluding to draw any conclusion.

Nanocomposite EVOH Films Reinforced with Plant Cellulose Nanowhiskers

With the purpose of comparing the effect of adding bacterial and plant CNW, films were produced by incorporating the latter ones through the precipitation method, obtaining final concentrations of 1, 2, and 3 wt % CNW. Additionally, the method of directly melt-mixing EVOH with freeze-dried CNW was also carried out for obtaining a film with 2 wt % CNW.

Morphological Characteristics of EVOH Nanocomposites with Plant-Derived CNW. The visual aspect of the obtained films is shown in Figure 10. As observed, no aggregates were detected in the films obtained by means of the precipitation method, although black spots, typical from thermal degradation, were present in the film obtained through direct melt-mixing of freeze-dried CNW. Just as observed for the BCNW, when increasing the nanowhiskers loading, the films got a yellowish color. When comparing the 2 wt % CNW FD-P film with the 2 wt % BCNW FD-P, the former appeared to be slightly darker, but it still showed a very good contact transparency.

As observed by SEM of cryofractured film sections, a good dispersion of the nanofiller was attained using the precipitation method, although small agglomerates were detected (see Figure 11A). The sizes of CNW's cross-sections were determined from SEM pictures of cryofractured surfaces and corresponded to 39 ± 16 nm, 60 ± 25 nm, and 139 ± 74 nm for the 1, 2, and 3% CNW FD-P, respectively. When comparing the 2% CNW FD-P with the film obtained exactly through the same incorporation method, that is, 2% BCNW FD-P, no significant differences were detected in the cross-section dimensions of the nanofiller.

Similarly to what was observed for the BCNW films, in the case of direct melt-mixing of the freeze-dried nanowhiskers, bundles were observed in the fractured section of the film (see Figure 11B). In this case, they presented a cross-section of 112 ± 63

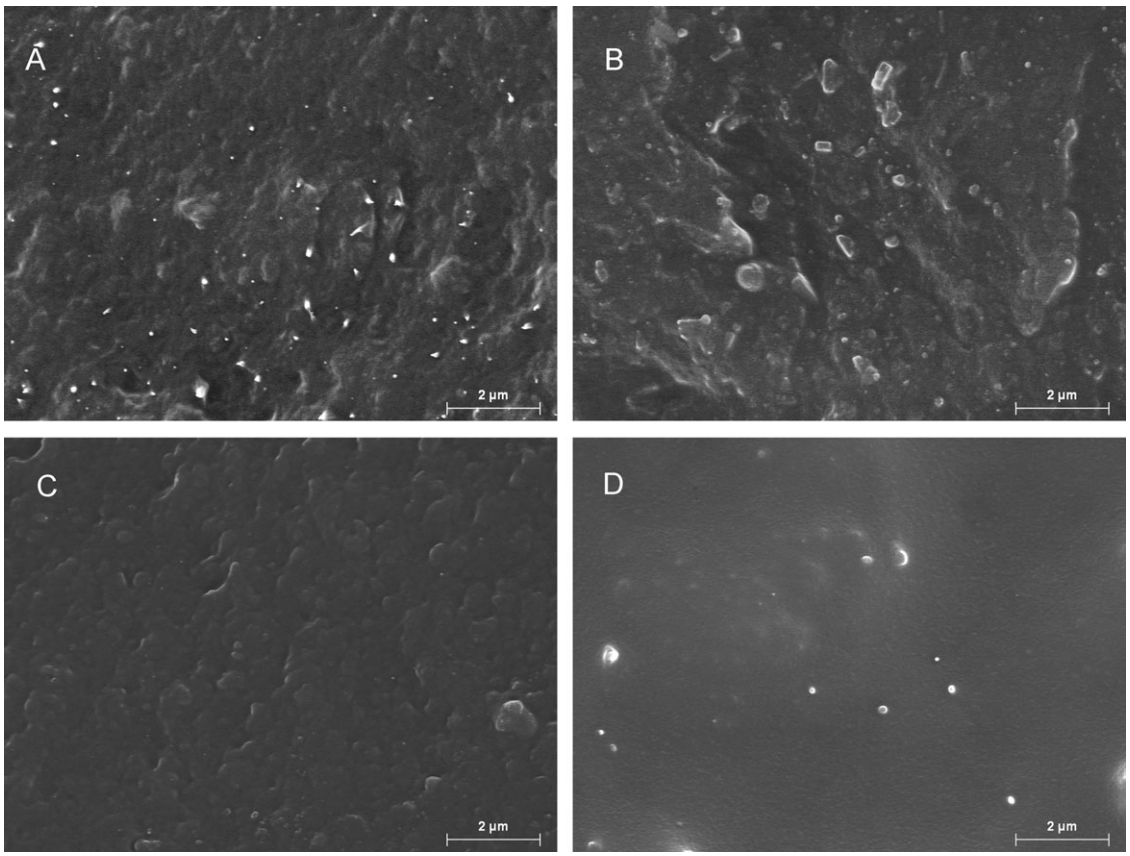

Figure 11. SEM micrographs of the cryofractured section obtained from films: (A) 2% CNW FD-P, (B) 2% CNW FD, (C) 1% CNW FD-P, and (D) 3% CNW FD-P. Scale markers correspond to 2 μm.

Table IV. DSC Maximum of Melting (T_m), Melting Enthalpy (ΔHm), Peak Width, and EVOH Crystallinity (X_c) of EVOH Films, Obtained During the First Heating Run and Glass Transition Temperature (T_g), Obtained During the Second Heating Run

	T_m (°C)	ΔH_m (J/g EVOH)	Peak width	X_c (%)	T_g (°C)
EVOH	177.7 ± 1.5	76.5 ± 0.1	7.1 ± 0.5	35.3 ± 0.0	59.5 ± 0.8
1% CNW P	177.6 ± 0.3	65.6 ± 0.7	7.7 ± 0.0	30.3 ± 0.3	58.9 ± 0.1
2% CNW P	178.0 ± 0.4	63.4 ± 1.2	6.1 ± 0.9	29.3 ± 0.5	60.5 ± 0.7
3% CNW P	178.0 ± 0.0	61.7 ± 5.0	7.5 ± 1.4	28.5 ± 2.3	60.3 ± 0.2
2% CNW FD	176.6 ± 0.1	66.8 ± 0.8	11.2 ± 4.9	30.9 ± 0.4	59.5 ± 0.1

nm and appeared to be much shorter than the ones observed in the BCNW film. The difference in the nanowhiskers length was probably due to the different production method used for each material. In the case of BCNW, they were obtained from the centrifugation precipitate, whereas CNW were recovered from the centrifugation supernatant where the shorter nanowhiskers are concentrated.

Thermal Properties of EVOH Nanocomposites with Plant-Derived CNW. Thermal properties of films incorporating CNW are gathered in Table IV. Although no significant differences were observed for the melting temperature and T_g of the nanocomposites obtained through the precipitation method, a slight decrease in the melting enthalpy of the materials was seen when increasing the CNW concentration. This could be related to the increased agglomeration observed when increasing the CNW loading, which led to a certain disruption of the EVOH crystalline phase. This effect was not observed for BCNW, because no significant agglomeration took place for the range of concentrations studied.

In contrast, a significant decrease in the melting temperature and melting enthalpy of the nanocomposite incorporating freeze-dried CNW was observed compared to the pure EVOH, because the agglomerated nanocrystals effectively distorted the EVOH crystalline network, resulting in smaller or more defective crystals. It is also worth noting the increase in peak width observed for this latter material, pointing out the greater heterogeneity of EVOH crystals present in the nanocomposite obtained through the traditional method.

CONCLUSIONS

In this first study, EVOH/CNW composite films were produced by melt-mixing, and the effects of the cellulose source, nanofiller concentration, and pre-incorporation method in the visual aspect, morphology, and thermal properties of the generated materials were investigated. Both bacterial and plant-derived CNW were used as nanofillers, being the cellulose source not a relevant factor for the degree of dispersion attained within the EVOH matrix. Non-hydrolyzed BC fibers were also used to generate nanocomposites, and, even though the size of the filler was considerably greater, a good dispersion was also seen. Most importantly, the method for incorporating the nanowhiskers before the melt compounding step largely determined the morphology of the obtained nanocomposites. Thus, except for the case of direct melt-mixing of the polymer with the freeze-dried nanomaterial, which resulted in agglomeration of the fillers, a homogeneous dispersion of the fillers was encountered using the two pre-incorporation strategies developed in this work.

In terms of thermal properties, the evidenced agglomeration observed for the films incorporating 2 wt % freeze-dried CNW and BCNW was reflected in a decrease in the melting temperature and melting enthalpy, indicating that non-homogeneously dispersed nanofiller hindered EVOH crystallization. The agglomeration effect observed when increasing the CNW loading, which was not observed for BCNW in the range screened, resulted in decreased crystallinity of the EVOH matrix as well. In the case of the nanocomposite containing BC, the bigger size of this filler also affected the thermal properties of the matrix decreasing both the temperature and enthalpy of fusion. These results evidence the adequacy of techniques such as electrospinning or precipitation using liquid nitrogen for the incorporation of CNW into EVOH matrices before a melt-mixing step in order to obtain EVOH nanocomposites showing a good dispersion of the cellulose fillers.

ACKNOWLEDGMENTS

M. Martínez-Sanz thanks the Spanish Ministry of Education for the FPU grant 1484. A. Lopez-Rubio is the recipient of a "Ramon y Cajal" contract from the Spanish Ministry of Science and Innovation. The authors acknowledge financial support from MICINN (MAT2009-14533-C02-01 project). Roxane Penades, on leave from the U. of Grenoble in France is acknowledged for her dedication and support in the experimental work related to plant cellulose nanowhiskers.

REFERENCES

1. Iguchi, M.; Yamanaka, S.; Budhiono, A. *J. Mater. Sci.* **2000,** *35*, 261.
2. Wan, Y. Z.; Huang, Y.; Yuan, C. D.; Raman, S.; Zhu, Y.; Jiang, H. J.; He, F.; Gao, C. *Mater. Sci. Eng. C* **2007,** *27*, 855.
3. Eichhorn, S. J.; Dufresne, A.; Aranguren, M.; Marcovich, N. E.; Capadona, J. R.; Rowan, S. J.; Weder, C.; Thielemans, W.; Roman, M.; Renneckar, S.; Gindl, W.; Veigel, S.; Keckes, J.; Yano, H.; Abe, K.; Nogi, M.; Nakagaito, A. N.; Mangalam, A.; Simonsen, J.; Benight, A. S.; Bismarck, A.; Berglund, L. A.; Peijs, T. *J. Mater. Sci.* **2010,** *45*, 1.
4. Araki, J.; Wada, M.; Kuga, S.; Okano, T. *Colloids Surf., Part A: Physicochem. Eng. Aspects* **1998,** *142*, 75.

5. Favier, V.; Chanzy, H.; Cavaille, J. Y. *Macromolecules* **1995,** *28*, 6365.
6. De Souza Lima, M. M.; Borsali, R. *Macromol. Rapid Commun.* **2004,** *25*, 771.
7. Hirai, A.; Inui, O.; Horii, F.; Tsuji, M. *Langmuir* **2009,** *25*, 497.
8. Petersson, L.; Kvien, I.; Oksman, K. *Compos. Sci. Technol.* **2007,** *67*, 2535.
9. Sanchez-Garcia, M. D.; Lagaron, J. M. *Cellulose* **2010,** *17*, 987.
10. Ten, E.; Turtle, J.; Bahr, D.; Jiang, L.; Wolcott, M. *Polymer* **2010,** *51*, 2652.
11. Kvien, I.; Sugiyama, J.; Votrubec, M.; Oksman, K. *J. Mater. Sci.* **2007,** *42*, 8163.
12. Petersson, L.; Mathew, A. P.; Oksman, K. *J. Appl. Polym. Sci.* **2009,** *112*, 2001.
13. Oksman, K.; Mathew, A. P.; Bondeson, D.; Kvien, I. *Compos. Sci. Technol.* **2006,** *66*, 2776.
14. Bondeson, D.; Oksman, K. *Compos., Part A: Appl. Sci. Manuf.* **2007,** *38*, 2486.
15. Bondeson, D.; Oksman, K. *Compos. Interf.* **2007,** *14*, 617.
16. Jiang, L.; Morelius, E.; Zhang, J.; Wolcott, M.; Holbery, J. *J. Compos. Mater.* **2008,** *42*, 2629.
17. Goffin, A. L.; Raquez, J. M.; Duquesne, E.; Siqueira, G.; Habibi, Y.; Dufresne, A.; Dubois, P. *Polymer* **2011,** *52*, 1532.
18. Blaker, J. J.; Lee, K. Y.; Mantalaris, A.; Bismarck, A. *Compos. Sci. Technol.* **2010,** *70*, 1879.
19. George, J.; Ramana, K. V.; Bawa, A. S.; Siddaramaiah, S. *Int. J. Biol. Macromol.* **2011,** *48*, 50.
20. George, J.; Siddaramaiah, S. *Carbohydr. Polym.* **2012**, *87*, 2031.
21. Martínez-Sanz, M.; Olsson, R.; Lopez-Rubio, A.; Lagaron, J. *J. Appl. Polym. Sci.* **2012,** *124*, 1398.
22. Martínez-Sanz, M.; Olsson, R. T.; Lopez-Rubio, A.; Lagaron, J. M. *Cellulose* **2011,** *18*, 335.
23. Olsson, R. T.; Kraemer, R.; Lopez-Rubio, A.; Torres-Giner, S.; Ocio, M. J.; Lagaron, J. M. *Macromolecules* **2010,** *43*, 4201.
24. Park, W. I.; Kang, M.; Kim, H. S.; Jin, H. *J. Macromol. Symp.* **2007,** 249–250, *289*.
25. Roman, M.; Winter, W. T. In ACS Symposium Series, Oskman, K. Sain, M., editors. American Chemical Society: Washington, DC; Vol. *938*; **2006;** pp 99–113.
26. Yun, Y. S.; Cho, S. Y.; Jin, H. *J. Mol. Crystals Liq. Crystals* **2010,** *519*, 141.
27. Yano, H.; Sugiyama, J.; Nakagaito, A. N.; Nogi, M.; Matsuura, T.; Hikita, M.; Handa, K. *Adv. Mater.* **2005,** *17*, 153.
28. Lagaron, J. M.; Martínez-Sanz, M.; Lopez-Rubio, A. *Pat. Appl.* P30663. (**2010**).
29. Lagaron, J. M.; Martínez-Sanz, M.; Lopez-Rubio, A. *Pat. Appl.* P31951 (**2011**).
30. Torres-Giner, S.; Gimenez, E.; Lagaron, J. M. *Food Hydrocoll.* **2008,** *22*, 601.
31. Wang, N.; Ding, E.; Cheng, R. *Polymer* **2007,** *48*, 3486.
32. Lagaron, J. M.; Gimenez, E.; Saura, J. J.; Gavara, R. *Polymer* **2001,** *42*, 7381.
33. Martínez-Sanz, M.; Lopez-Rubio, A.; Lagaron, J. *Carbohydr. Polym.* **2011,** *85*, 228.
34. Bondeson, D.; Mathew, A.; Oksman, K. *Cellulose* **2006,** *13*, 171.
35. Moharram, M. A.; Mahmoud, O. M. *J. Appl. Polym. Sci.* **2007,** *105*, 2978.
36. Elanthikkal, S.; Gopalakrishnapanicker, U.; Varghese, S.; Guthrie, J. T. *Carbohydr. Polym.* **2010,** *80*, 852.
37. Wong, S.-S.; Kasapis, S.; Tan, Y. M. *Carbohydr. Polym.* **2009,** *77*, 280.
38. Roman, M.; Winter, W. T. *Biomacromolecules* **2004,** *5*, 1671.
39. Filson, P. B.; Dawson-Andoh, B. E. *Bioresour. Technol.* **2009,** *100*, 2259.
40. Oh, S. Y.; Yoo, D. I.; Shin, Y.; Seo, G. *Carbohydr. Res.* **2005,** *340*, 417.
41. Ayuk, J. E.; Mathew, A. P.; Oksman, K. *J. Appl. Polym. Sci.* **2009,** *114*, 2723.
42. Carrillo, F.; Colom, X.; Suñol, J. J.; Saurina, J. *Eur. Polym. J.* **2004,** *40*, 2229.
43. Lagaron, J. M.; Gimenez, E.; Catala, R.; Gavara, R. *Macromol. Chem. Phys.* **2003,** *204*, 704.
44. Peresin, M. S.; Habibi, Y.; Zoppe, J. O.; Pawlak, J. J.; Rojas, O. *J. Biomacromolecules* **2010,** *11*, 674.
45. Anglès, M. N.; Dufresne, A. *Macromolecules* **2001,** *34*, 2921.
46. Qua, E. H.; Hornsby, P. R.; Sharma, H. S. S.; Lyons, G.; McCall, R. D. *J. Appl. Polym. Sci.* **2009,** *113*, 2238.
47. Samir, M. A. S. A.; Alloin, F.; Sanchez, J. Y.; Dufresne, A. *Polymer* **2004,** *45*, 4149.